Hindawi
International Journal of Polymer Science
Volume 2018, Article ID 1067902, 7 pages
https://doi.org/10.1155/2018/1067902

Research Article

Research of Flow Field of Alkaline/Surfactant/Polymer Solution in the Annular Depressurization Slot by PIV Experiment

Cheng Fu,[1,2] Tingting Zhu,[1] Di Wu,[3] Ying Wang,[4] and Bin Huang[1]

[1]*College of Petroleum Engineering, Northeast Petroleum University, China*
[2]*Post-Doctoral Scientific Research Station, Daqing Oilfield Company, China*
[3]*Hangzhou Urban & Rural Construction Design Institute Limited Company, China*
[4]*Aramco Asia, China*

Correspondence should be addressed to Bin Huang; huangbin502a@163.com

Received 27 July 2017; Revised 14 November 2017; Accepted 13 September 2018; Published 3 December 2018

Academic Editor: Domenico Acierno

In order to study the flow field changes of ASP (alkaline/surfactant/polymer) solutions with different molecular weights and flow rates when flowing through the annular depressurization slot in the laboratory, the annulus pipeline model was designed based on the principle of similarity. The particle image velocimetry (PIV) system was used to continuously capture the transient images when the ASP solution flows in the model under different experimental conditions. Tecplot software was used to analyze and process the nephrograms of the velocity distribution of ASP solution when flowing through the partially pressured injection tool with different depressurization slots. The experimental results showed that the vortex occurred at the bottom of the depressurization slots; the greater the flow rate, the closer the vortex center to the outer wall; higher molecular weight of the polymer in the ASP solution caused larger velocity gradient towards the wall. The number of the slots has no significant effect on the position of the vortex. This experiment provides a new research method for the velocity distribution of the internal flow field in the partially pressured injection tool.

1. Introduction

In past years, the application of the partially pressured injection tool used in Indonesia Limau oil has been limited due to a lack of sufficient theoretical basis for the runner shape design. This also restricted the design and manufacture of pressure relief groove. Therefore, studying the internal flow field of the partially pressured injection tool is necessary [1, 2].

Compared with the point measurement by Laser Doppler Velocimetry (LDV), PIV can perform direct surface measurements for the flow field to ensure the accuracy of the measurement and certain spatial resolution. Therefore, PIV is suitable to analyze the change of the flow field. PIV has two distinct characteristics: it does not disturb the flow field and the entire picture of the flow field can be simultaneously obtained through instantaneous flow-velocity vector. It is a powerful tool to study complex flow structures such as eddy currents and turbulence [3–5].

Feng et al. [6] simulated the flow process and flow field of the polymer solution through the layered injector and found that the flow of the polymer in the layered injector was relatively stable. This could be a benefit for preventing the mechanical shearing and reducing the viscosity loss of the polymer solution during the polymer injection process. Meng et al. [7] used the software PHOENICS to calculate the flow field in the layered injector and found that the shape of the annular channel of the layered injector had great influence on the flow field characteristics. Cai et al. [8] analyzed the flow field of the ASP solution in the eccentric injector by the commercial software Fluent. The simulation results showed that the velocity and pressure of the flow were periodic, and each period was similar. Due to a lack of experimental methods, the optimization of the structure of

the partially pressured injection tool and the flow-field distribution in the depressurization slot of the injection tool were mainly simulated and analyzed by using Fluent numerical simulation software. Our research is the first trial to study the flow field of the injection tool by experimental method.

In this paper, the interior flow field of the injection tool is studied by laboratory experiments. A set of experimental models of partially pressured injection tools for PIV system are designed by using the principle of similarity [9–11]. Three experiments with different flow rate, component, and number of slots were performed and compared with the experimental model [12]. A high-speed camera was used to capture the images of the flow field within the partially pressured injection tool. Different postprocessing had been used to handle the experimental data by Tecplot software. The flow field conditions within the partially pressured injection tool had been determined under different experimental conditions. The influence regulations for the inner flow field of the polymer with the weak base have been obtained for three element solutions with different molecular weight, flow rate, and number of slots. It will help provide guidance for the design of the depressurizing channel in the future.

2. The Principle of Similarity

2.1. Similar Proportions

2.1.1. Geometric Similarity. The shape of the model used in this experiment is exactly the same as the prototype of the partially pressured injection tool. In order for good quality observations, the model was enlarged to a certain proportion [13]. Assuming that the length of the depressurization slot in the model is l_m, the diameter is D_m, and the length of the actual depressurization slot of the partially pressured injection tool is l_p, the diameter is D_p.

The proportion of geometric similarity is expressed as

$$\lambda_l = \frac{l_p}{l_m} = \frac{D_p}{D_m}. \tag{1}$$

2.1.2. Kinematic Similarity. Under similar geometrical conditions, the scale of time can be described as

$$\lambda_l = \frac{l_p}{l_m} = \frac{D_p}{D_m}, \tag{2}$$

and the scale of velocity can be described as

$$\lambda_v = \frac{v_p}{v_m} = \frac{l_p/t_p}{l_m/t_m} = \frac{\lambda_l}{\lambda_t}, \tag{3}$$

where v is the average velocity when the solution flows through the depressurization slot; t is the time for the solution to pass through the length l of the depressurization slot.

2.1.3. Dynamic Similarity. The scale of pressure can be described as

$$\lambda_F = \frac{F_p}{F_m} = \frac{m_p a_p}{m_m a_m} = \frac{\rho_p V_p a_p}{\rho_m V_m a_m} = \lambda_\rho \lambda_l{}^2 \lambda_v{}^2. \tag{4}$$

The solution used in the experiment is the same as that used in the field. It means that ρ_p is equal to ρ_m. Therefore, the following formulation can be obtained:

$$\lambda_F = \lambda_l{}^2 \lambda_v{}^2. \tag{5}$$

2.2. Criterion of Similarity. Since the viscous force plays an important role in this experiment, the criterion of similarity for viscous force is used to judge similar situations. The similitude criterion of the viscous force is the Reynolds number. Therefore, if the Reynolds number of the prototype is equal to the model, the dynamic similarity can be achieved.

The generalized Reynolds number of non-Newtonian fluid can be described as

$$\mathrm{Re}' = \frac{Dv\rho}{K'(8v/D)^{n'-1}} = \frac{D^{n'} v^{2-n'} \rho}{8^{n'-1} K'}. \tag{6}$$

The equation can be concluded by calculating as follows:

$$K' = K\left(\frac{3n+1}{4n}\right)^n, \tag{7}$$

where the value of n is equal to the value of n', namely,

$$\mathrm{Re} = \frac{D^n v^{2-n} \rho}{8^{n-1} K((3n+1)/4n)^n} = \frac{D^n v^{2-n} \rho}{K/8((6n+2)/n)^n}. \tag{8}$$

The experiment needs to

$$\frac{\mathrm{Re}_p}{\mathrm{Re}_m} = \frac{v_p d_p \rho_p}{v_m d_m \rho_m} = 1. \tag{9}$$

Because the cross section of the model is a concentric circle and the hydraulic diameter of the model is the characteristic length of the model. The characteristic length can be described as follows:

$$R_h = \frac{A}{\chi} = \frac{4\pi\left(R^2 - \bar{r}^2\right)}{\chi} = \frac{4\pi\left(R^2 - \bar{r}^2\right)}{2\pi(R + \bar{r})} = 2(R - \bar{r}). \tag{10}$$

Where χ is the wetted perimeter, A is the cross section area of passage, R is the outer radius of the flow section, and $\bar{r}$ is the inner radius of the flow section.

Since $G = v \cdot A$, $A = 4\pi(R^2 - \bar{r}^2)$ the following are obtained:

$$\frac{\mathrm{Re}_p}{\mathrm{Re}_m} = \frac{G_p d_p \rho_p / A_p}{G_m d_m \rho_m / A_m} = \frac{G_p/\chi_p}{G_m/\chi_m} = \frac{G_p/\left(R_p + \bar{r}_p\right)}{G_m/(R_m + \bar{r}_m)} = 1. \tag{11}$$

Figure 1: Geometric structure of streamlined partially pressured injection tool.

Figure 2: Modified shuttle rod partially pressured injection tool.

When the ratio of the flow rate of the experimental model vs. the field condition reaches the above conditions, the dynamic similarity can be considered.

2.3. Streamlined Partially Pressured Injection Tool. The main objective of the simulation research is to optimize the internal structure of the depressurizing channel in the streamlined partially pressured injection tool. The structure of streamlined-separating injection tool is shown in Figure 1, and the modified shuttle rod partially pressured injection tool is shown in Figure 2.

As shown in Figures 1 and 2, the depressurizing channel is a solid column in the middle with a waveform. By changing the cross-sectional area of the channel, a casing pipe allows the solution to flow through the gap to cause pressure loss so as to achieve the aim of reducing pressure. The various structure parameters such as slot length and slot distance of the injection tools with differential pressure type flow are suitable for different conditions.

2.4. Experimental Models. In order to ensure good quality particle image, the acrylic material was used to prepare the experiment model. The size of the depressurization slot is shown in Figure 3.

3. Experimental Scheme and Procedure

3.1. Solution Compositions. In this experiment, the water for the polymer solution was synthetic brine (the salinity was 6778 mg/L). The surfactant was 0.3% alkylbenzene sulfonate. The weak alkali was 1.2% Na_2CO_3. The polymer was polyacrylamide (HPAM) produced in Daqing Refinery and Chemical Company with molecular weights of 1.6×10^6, 1.9×10^6, and 2.5×10^6, respectively.

3.2. Experimental Setup. The PIV used in the experiment was MiniPIV. The exposure time of high-speed camera was 1/128000 sec. The tracer particle was hollow glass bead ($d \leq 10$ μm, 0.1 g/L).

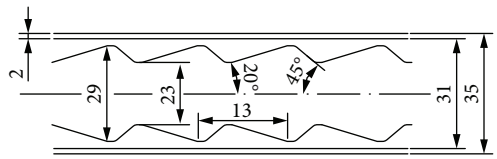

Figure 3: The size of the depressurizing channel in the experimental model.

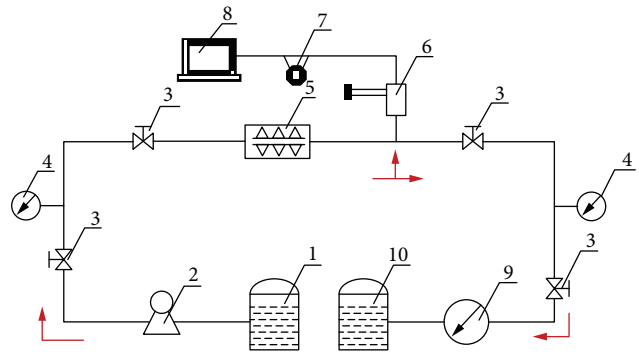

Figure 4: Schematic diagram of the experiment setup. 1 liquid storage tank, 2 screw pump, 3 valve, 4 pressure gauge, 5 injection tool model, 6 laser emitter, 7 camera, 8 data processing system, 9 flow meter, and 10 return liquid tank.

Figure 4 shows the schematic diagram of the experimental setup. All the experiments were carried out in a room with no interference from light source.

The camera in Figure 4 captures images of the solution in a reciprocal second slot of the depressurizing channel in Figure 1. It is a high-speed camera and part of PIV system. In the experiment, at least 100 images of the flow field should be continuous shot with the middle 50 images were selected to do cross-correlation calculation. Then, the vector files were poured into Tecplot 10.0 software, and finally, the velocity nephograms were generated with shooting accuracy of 0.01.

3.3. Experiment Schemes. A total of 3 groups of PIV test were carried out for the same molecular weight, flow rate, and the number of depressurization slots of the model. The experiment schemes are shown in Table 1.

3.4. Experimental Procedures. The experimental steps are as follows:

(1) Connect the experimental setup as shown in Figure 4

(2) Make the polymer solutions which were used in the experiment and add the tracer particles

Table 1: Experimental schemes of the PIV test.

	Polymer molecular weight	Polymer concentration (mg/L)	Flow rate (m^3/d)	Number of slots
Scheme 1	1.6×10^6 1.9×10^6 2.5×10^6	2000	30	18
Scheme 2	1.6×10^6	2000	20 30 50	18
Scheme 3	1.6×10^6	2000	30	5 10 18

Table 2: Viscosity of ASP solution.

	Polymer molecular weight	Polymer concentration (mg/L)	Solution viscosities (mPa·s)
Scheme 1	1.6×10^6	2000	42.3
Scheme 2	1.9×10^6		45.6
Scheme 3	2.5×10^6		51.4

(3) Start the experiment and photograph the images of the solution flowing in a depressurization slot

(4) Analyze the collected images using the Tecplot software

3.5. Solution Viscosity. The relationship between viscosity and concentration of the polymer in the ASP systems are listed in Table 2.

According to Table 2, the molecular weight of the polymer has a significant effect on the viscosity of ASP system. With the increase of polymer molecular weight, the viscosity of the ASP system increased.

4. Experimental Results and Analysis

4.1. Velocity Nephograms. The velocity nephograms of different molecular weight, flow rate, and number of slots (the length of the depressurizing channel increases with the number of slots) were obtained by the Tecplot software which are shown in Figures 5–7. The different colors in the velocity nephograms represent different speeds. For the same graph, red color indicates maximum speed and the blue color indicates zero velocity.

From Figure 5, the maximum velocity appears at the minimum clearance of the annular. The overall flow directions of the solution are the same. This is due to the minimum flow area of the decompression slot in the partially pressured injection tool, where the flow rate of the solution is constant with the greatest flow velocity at that point. As the solution continues to flow in the partially pressured injection tool, the flow area in the pressure-reducing groove increases gradually, resulting in the velocity decreasing gradually. The flow direction of the solution gradually spreads to the center of the pressure reducing groove. At about 3/4 slot length, the flow rate gradually increased and the direction of flow gather up again. The reason for that is as the solution in the decompression slot continues to move forward, the flow cross-sectional area becomes smaller, thus the liquid flow velocity increased gradually. The clockwise vortex is formed at the center of the pressure reducing groove with the minimum velocity at the center of the vortex and gradually increasing towards the channel wall.

From Figure 5, it can be concluded that the greater the viscosity of the solution, the greater the velocity around the vortex will be, especially below the vortex, and the smaller the axial velocity gradient at the top of the vortex.

From Figure 6, as the flow rate of the weak base ASP solution flows through the partially pressured injection tool decreased, the center of the vortex approached more to the left; the higher the flow rate caused the center in the groove of the vortex offset more away from the right.

As can be observed from Figure 7, with the same flow rate and composition, by changing the number of slot, the vortex position and velocity distribution change is not obvious.

4.2. The Distribution Images of the Axial Velocity. The velocity distributions of different polymer molecular weight are shown in Figure 8. The cutline represents the distance between the bushing and the bottom of the depressor trough of 10 mm, 23 mm, 32 mm, 37 mm, 40 mm, and 42 mm, respectively.

Figure 8 shows that, for weak base ASP solution with larger molecular weight when flowing through the partially pressured injection tool, the flow rate becomes smaller when approaching to the outer wall of the pressure injection tool but bigger in the bottom. With the decrease of the molecular weight of the polymer in solution, the smaller the velocity gradient is, the smaller the difference of the velocity of the solution with adjacent height will be. At the same time, the maximum velocity at the minimum gap of the annulus decreases with the increase of molecular weight of the polymer. The velocity gradient at the minimum clearance of the annulus increases with the increase of molecular weight of the polymer in weak base ASP system.

The velocity distribution of different flow rate is shown in Figure 9.

From Figure 9, the velocity is less, and the flow rate variation of the solution near the outer wall is greater than that at the center of the annulus gap of the pressure relief groove. With the decrease of the flow rate of the pressure injection tool, the location where the velocity changes from a decrease to an elevation shifts gradually to the right. The flow rate in the buck groove bottom is greater than that at the center of the vortex. The closer to the center of the pressure relief groove, the lower the velocity will be. With the buck groove bottom near the inner wall, the velocity changes from increase to decrease, which is due to the viscous force in the partially pressured injection tool device. In addition, when the flow rate is low, the change of flow velocity at the groove is more obvious.

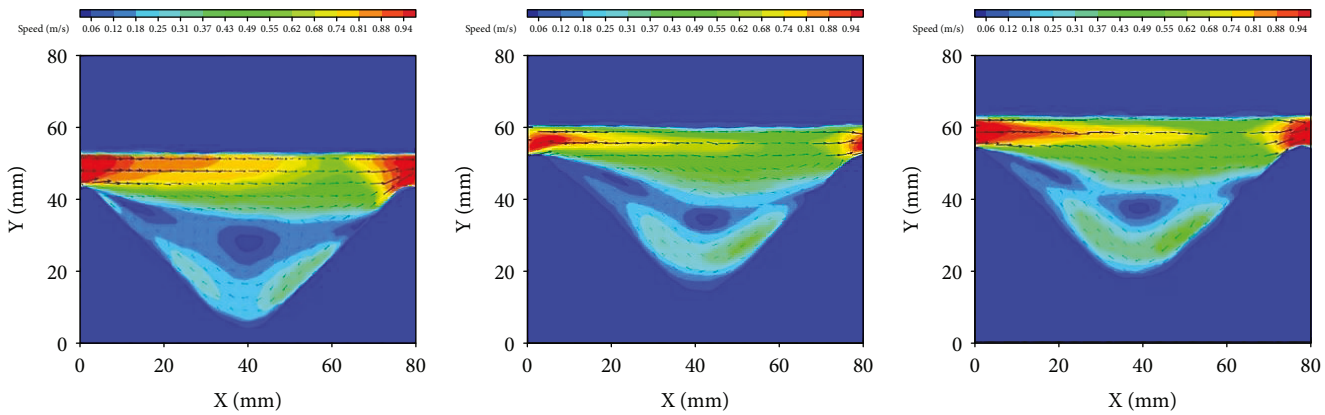

(a) 1.6×10^6 dalton (b) 1.9×10^6 dalton (c) 2.5×10^6 dalton

Figure 5: Velocity nephograms of different polymer molecular weight when flowing through the partially pressured injection tool.

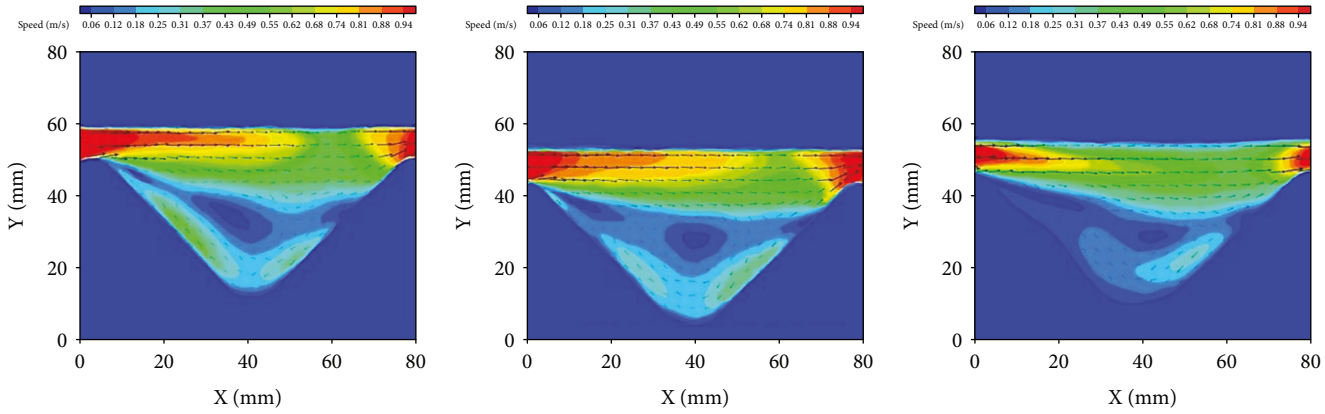

(a) 20 m^3/d (b) 30 m^3/d (c) 50 m^3/d

Figure 6: Velocity nephograms of different flow rate of polymer solution flowing through the partially pressured injection tool.

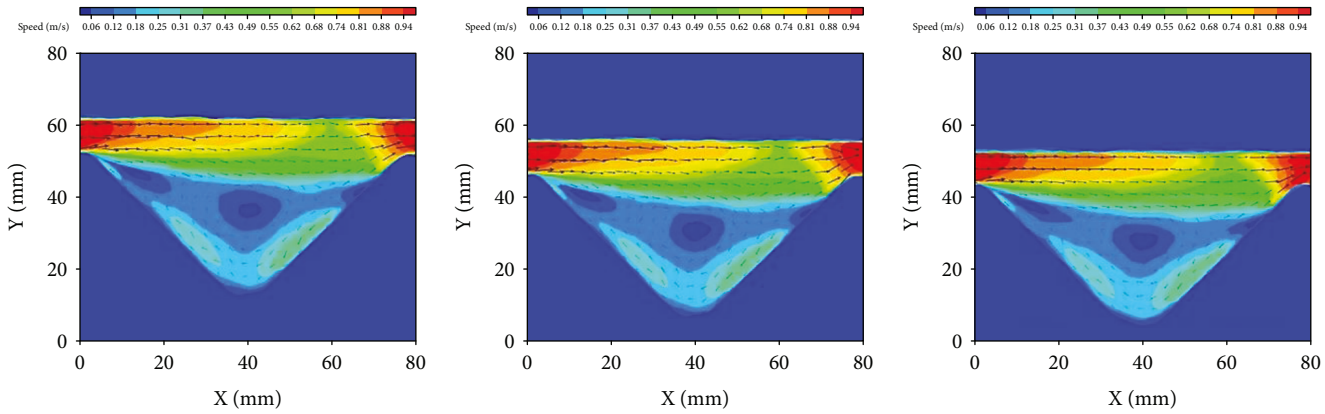

(a) 5 pressure reduction trough (b) 10 pressure reduction trough (c) 18 pressure reduction trough

Figure 7: Velocity nephograms of the polymer solution that flowed through the partially pressured injection tool with different number of slots.

The velocity distribution of different number of slots are shown in Figure 10.

The same can be seen from Figure 11. When the weak base ASP solution with the same composition and velocity flows through the partially pressured injection tool with different slots, the change of the end groove of the flow field is not obvious. Comparing to Figure 10, the velocity difference at the relative position is very small. The reason is that the partially pressured injection tool device has a shearing action to the weak base ASP solution. Therefore, the viscosity changes slightly leading to the internal flow field changes. However, the change was not obvious.

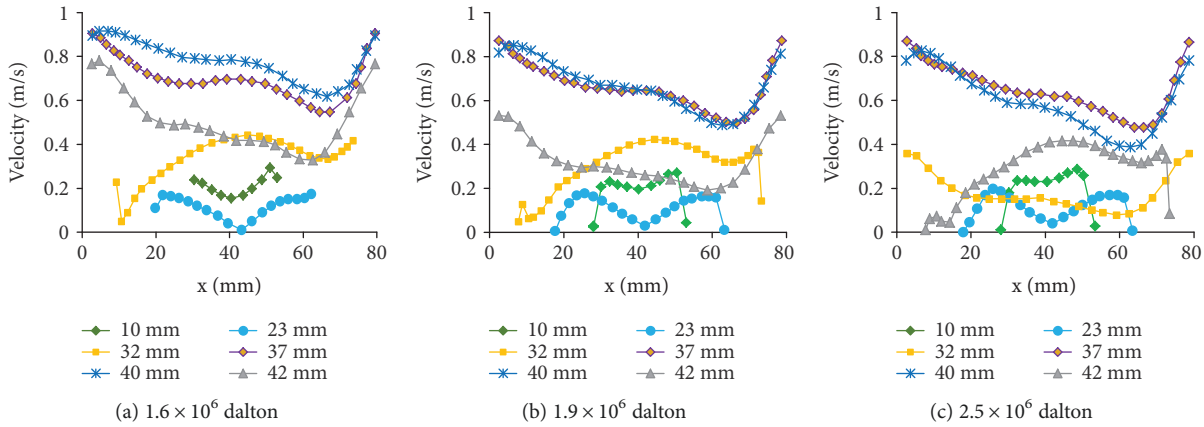

Figure 8: Velocity distribution of the polymer solution at 30 m^3/d through the partially pressured injection tool with 18 slots.

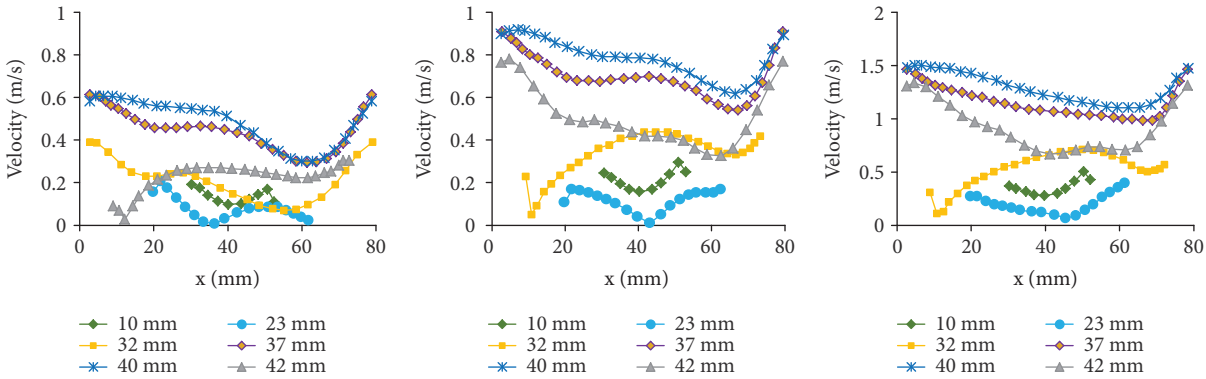

Figure 9: Velocity distribution of the polymer solution with a molecular weight of 1.6×10^6 dalton at 50 m^3/d when flowing through the partially pressured injection tool with 18 slots.

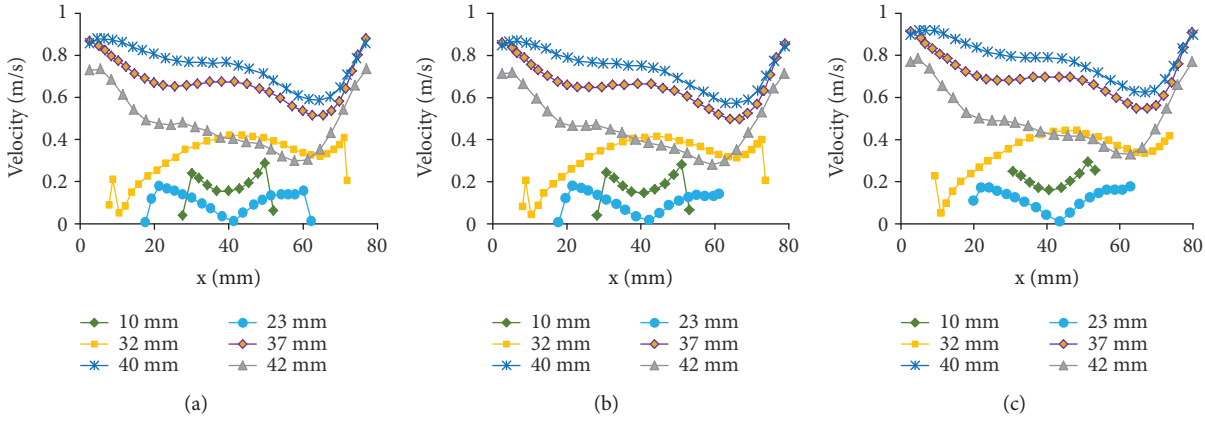

Figure 10: Velocity distribution of the polymer solution with a molecular weight of 1.6×10^6 dalton at 50 m^3/d when flowing through the partially pressured injection tool with 5 slots.

5. Conclusions

(1) The similarity between the experimental model and the prototype was analyzed. The experimental model was designed based on the theory of similarity.

(2) Using PIV system and Tecplot software, the flow-field distribution of the polymer solution was obtained for different flow rates, molecular weight polymer, and number of slots. It can provide the basis for optimization of the flow-channel structure in the future.

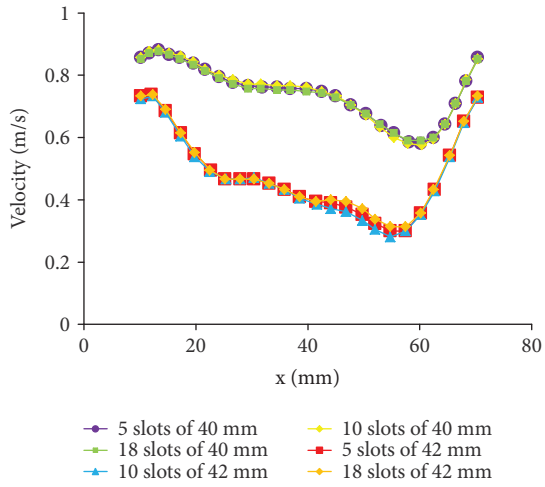

Figure 11: Contrast chart of flow velocity under different number of slots.

(3) The viscosity and flow rate of the solution have a significant influence on the velocity distribution in the depressurization slot. The effect of the slot number on the velocity distribution is not obvious.

(4) In this paper, the flow field inside the depressurizing channel of the partially pressured injection tool was studied. The variation rules under different working conditions were analyzed so as to design and optimize the structure of the depressurizing channel in the partially pressured injection tool in the future.

Conflicts of Interest

The authors declare that they have no conflicts of interest.

Acknowledgments

This work is financially supported by the Science and Technology Research Project of Heilongjiang Education Department (No. 12541092).

References

[1] H. C. Li, "Overview of separate injection technique for polymerflooding in Daqing oilfield," *Oil and Gasgeology*, vol. 33, no. 2, pp. 296–301, 2012.

[2] C. Ruan, "The characteristics of the tracer particles used in water flow field for PIV system," *Journal of Experiments in Fluid Mechanics*, vol. 20, no. 2, pp. 72–77, 2006.

[3] D. Wu, "Structural optimization and internal flow field analysis of the mass separate injection tool for weak base ASP solution," Northeast Petroleum University, Daqing, China, 2017.

[4] L. Wang, "Polymer separate injection technology with separate mass and pressure," *Oil Drilling & Production Technology*, vol. 29, no. 2, pp. 73–75, 2007.

[5] X. H. Chen, "Principle and application of polymer single tube multilayer separate injection technique," *Petroleum Geology and development in Daqing*, vol. 23, no. 4, pp. 53–55, 2004.

[6] D. Feng, X. M. Li, and C. B. Huang, "Research on the flow of the annular polymer in separate-layer polymer injection allocator," *Petroleum Machinery*, vol. 37, no. 10, pp. 7–10, 2009.

[7] L. Z. Meng, H. Q. Cui, and C. B. Wang, "Numerical simulation for corrugation and annular flow field of a stratification injection allocator," *Petroleum Machinery*, vol. 34, no. 2, pp. 15–17, 2006.

[8] M. Cai, Y. Sun, and L. D. Liu, "The flow flied numerical analysis of ternary composite solution in eccentric injection allocation device flows through the nozzle," *Oil Production Engineering*, vol. 3, no. 1, pp. 12–16, 2013.

[9] T. Schmitt, J. N. Koster, and H. Hamacher, "Particle design for displacement tracking velocimetry," *Measurement Science and Technology*, vol. 6, no. 6, pp. 682–689, 1995.

[10] A. Melling, "Tracer particles and seeding for particle image velocimetry," *Measurement Science and Technology*, vol. 8, no. 12, pp. 1406–1416, 1997.

[11] R. Y. Zhang, "Technologies of separated layer water flooding: an overview," *Oil Drilling and Production Technology*, vol. 33, no. 2, pp. 102–107, 2011.

[12] F. S. Wang, "Based on the technology of PIV flow field characteristics of the research in layered injection tools and experiment comparison," *Oil Field Equipment*, vol. 45, no. 6, pp. 16–19, 2016.

[13] S. R. Yang, *Engineering Fluid Mechanics*, Petroleum Industry Press, Beijing, 2006.